

Structure effect on intrinsic piezoelectricity in septuple-atomic-layer MSi_2N_4 (M=Mo and W)

San-Dong Guo¹, Yu-Tong Zhu¹, Wen-Qi Mu¹, Lei Wang^{2,3} and Xing-Qiu Chen^{2,3}

¹*School of Electronic Engineering, Xi'an University of Posts and Telecommunications, Xi'an 710121, China*

²*Shenyang National Laboratory for Materials Science, Institute of Metal Research, Chinese Academy of Science, 110016 Shenyang, Liaoning, P. R. China and*

³*School of Materials Science and Engineering, University of Science and Technology of China, Shenyang 110016, P. R. China*

The recently experimentally synthesized monolayer MoSi_2N_4 and WSi_2N_4 (Science 369, 670-674 (2020)) lack inversion symmetry, which allows them to become piezoelectric. In this work, based on ab initio calculations, we report structure effect on intrinsic piezoelectricity in septuple-atomic-layer MSi_2N_4 (M=Mo and W), and six structures (α_i ($i=1$ to 6)) are considered with the same space group. These structures can connect to each other through translation, mirror and rotation operations of double layer unit Si_2N_2 . It is found that MSi_2N_4 (M=Mo and W) with α_i ($i=1$ to 6) all are indirect band gap semiconductors. Calculated results show that MoSi_2N_4 and WSi_2N_4 monolayers have the same structural dependence on piezoelectric strain and stress coefficients (d_{11} and e_{11}), together with the ionic and electronic contributions to e_{11} . The α_5 phase has largest d_{11} for both MoSi_2N_4 and WSi_2N_4 , which are larger than 2.9 pm/V. Finally, we investigate the intrinsic piezoelectricity of monolayer MA_2Z_4 (M=Cr, Mo and W; A=Si and Ge; Z=N and P) with α_1 and α_2 phases except CrGe_2N_4 , because they all are semiconductors and their enthalpies of formation between α_1 and α_2 phases are very close. The most important result is that monolayer MA_2Z_4 containing P atom have more stronger piezoelectric polarization than one including N atom. The largest d_{11} among MA_2N_4 materials is 1.85 pm/V, which is close to the smallest d_{11} of 1.65 pm/V in MA_2P_4 monolayers. For MA_2P_4 , the largest d_{11} is up to 6.12 pm/V. Among the 22 monolayers, α_1 - CrSi_2P_4 , α_1 - MoSi_2P_4 , α_1 - CrGe_2P_4 , α_1 - MoGe_2P_4 and α_2 - CrGe_2P_4 have large d_{11} , which are greater than or close to 5 pm/V, a typical value for bulk piezoelectric materials. These materials are recommended for experimental exploration. Our study reveals that the MA_2Z_4 family have the potential applications in piezoelectric field.

PACS numbers: 71.20.-b, 77.65.-j, 72.15.Jf, 78.67.-n

Keywords: MA_2Z_4 family, Piezoelectronics, 2D materials

Email:sandongyuwang@163.com

I. INTRODUCTION

In semiconductors or insulators with broken inversion symmetry, an intrinsic electromechanical coupling between stresses and electric polarizations can be observed, which is called piezoelectric effect. Two-dimensional (2D) materials can show unique properties compared to their bulk counterparts, and the reduction in dimensionality of 2D materials can often eliminate inversion symmetry, which allows these materials to become piezoelectric¹. It has been theoretically reported that many 2D materials break inversion symmetry and hence can exhibit piezoelectricity, such as group IIA and IIB metal oxides, group-V binary semiconductors, transition metal dichalcogenides (TMD), Janus TMD and group III-V semiconductors²⁻¹³. A majority of structures have piezoelectric coefficients greater than a typical value of bulk piezoelectric materials (5 pm/V). Significantly, the monolayer SnSe, SnS, GeSe and GeS with puckered structure possess giant piezoelectricity, as high as 75-251 pm/V⁸, which may have huge potential application in the field of sensors, actuators and energy harvesters. The different crystal symmetry can induce a only in-plane piezoelectricity like TMD monolayers⁷, both in-plane and out-of-plane piezoelectricity for example 2D Janus monolayers^{2,4}, or a pure out-of-plane piezoelectricity such as penta-graphene¹⁴. It has been proved that

strain may be a effective strategy to tune piezoelectric properties of 2D materials^{15,16}. Experimentally discovered piezoelectricity of MoS_2 ^{17,18}, MoSSe ¹⁹ and In_2Se_3 ²⁰ has triggered an intense interest in piezoelectric properties of 2D materials.

It is meaningful to explore piezoelectricity of new 2D family. Recently, the layered 2D MoSi_2N_4 has been experimentally achieved by chemical vapor deposition (CVD)²¹, which possesses semiconducting behavior, high strength and excellent ambient stability. In rapid sequence, 2D WSi_2N_4 has also been synthesized by CVD. In the wake of MSi_2N_4 (M=Mo and W), MA_2Z_4 family are constructed with twelve different structures (α_i and β_i ($i=1$ to 6)) by intercalating MoS_2 -type MZ_2 monolayer into InSe-type A_2Z_2 monolayer²². The MA_2Z_4 family spans a wide range of properties from semiconductor to topological insulator to Ising superconductor upon the number of valence electrons (VEC). Intrinsic piezoelectricity in monolayer XSi_2N_4 (X=Ti, Zr, Hf, Cr, Mo and W) with α_1 phase are studied by the first principle calculations²³, and the independent in-plane piezoelectric constants d_{11} is predicted to be 0.78 pm/V-1.24 pm/V. The valley-dependent properties of monolayer MoSi_2N_4 , WSi_2N_4 and MoSi_2As_4 have been investigated by the first-principle calculations²⁴. The structural, mechanical, thermal, electronic, optical and photocatalytic properties of MoSi_2N_4 are studied by using hybrid density

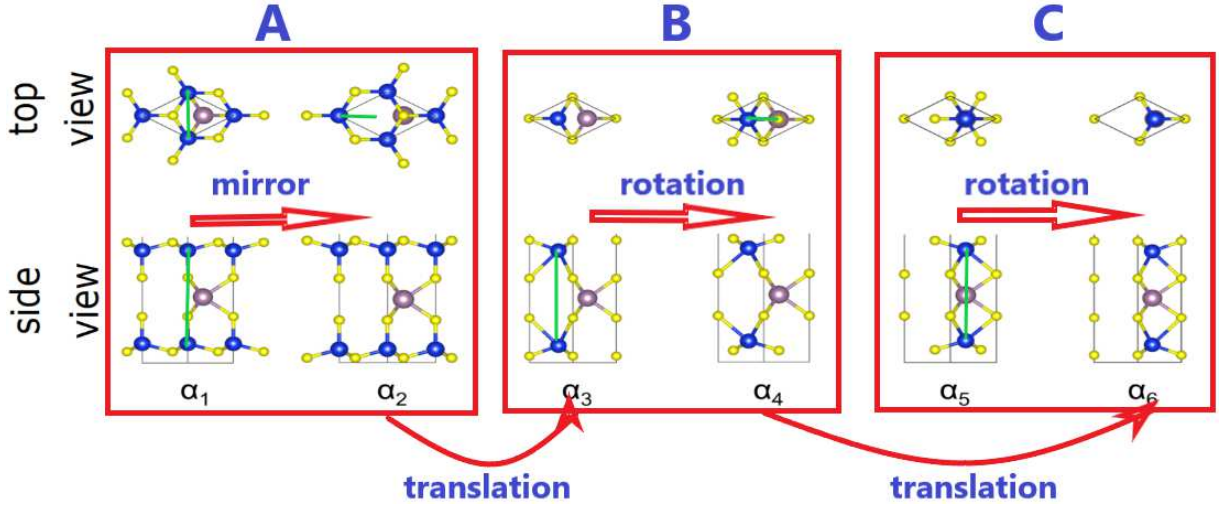


FIG. 1. (Color online) The crystal structure of α_i - ($i=1$ to 6) MA_2Z_4 including top and side views. The purple balls represent M atoms, and the blue balls for A atoms, and the yellow balls for Z atoms. These crystal structure can be divided into three categories: A (α_1, α_2), B (α_3, α_4) and C (α_5, α_6) according to the relative positions of M and A atoms. The different categories can be connected by translation operation, and the different structures in the same category can be related by mirror or rotation operations. The green lines represent mirror face, translation direction or rotation axis.

TABLE I. The optimized lattice constants of α_i - ($i=1$ to 6) MSi_2N_4 (M=Mo and W) using GGA (\AA).

Name	α_1	α_2	α_3	α_4	α_5	α_6
MoSi ₂ N ₄	2.91	2.90	2.84	2.84	2.86	2.85
WSi ₂ N ₄	2.91	2.90	2.84	2.84	2.87	2.85

functional theory (HSE06-DFT)²⁵.

In this work, the role of crystal structure on intrinsic piezoelectricity in monolayer MSi_2N_4 (M=Mo and W) are studied by using density functional perturbation theory (DFPT)²⁶. It is interesting to note that the same structural dependence on d_{11} and e_{11} between monolayer MoSi₂N₄ and WSi₂N₄ is observed. Calculated results show that the atomic arrangement of A_2Z_2 double layers has important effect on the in-plane piezoelectric polarization of MSi_2N_4 (M=Mo and W) monolayers. Finally, we investigate the intrinsic piezoelectricity of monolayer α_1 - and α_2 - MA_2Z_4 (M=Cr, Mo and W; A=Si and Ge; Z=N and P) expect CrGe₂N₄. It is found that the MA_2P_4 have more stronger piezoelectricity than MA_2N_4 . So, experimentally synthesizing monolayer MA_2Z_4 containing P atoms is very promising for energy harvesting and piezoelectric sensing.

The rest of the paper is organized as follows. In the next section, we shall give our computational details and methods about piezoelectric coefficients. In the third section, we perform symmetry analysis for elastic and piezoelectric coefficients of α_i - ($i=1$ to 6) MA_2Z_4 . In the fourth sections, we shall present main results and analysis. Finally, we shall give our conclusions in the fifth section.

II. COMPUTATIONAL DETAIL

Based on the density functional theory (DFT)²⁷, our simulations are carried out as implemented in the plane-wave code VASP²⁸⁻³⁰. The exchange-correlation functional is treated within popular generalized gradient approximation of Perdew, Burke and Ernzerhof (GGA-PBE)³¹ to perform the structural relaxation and the calculations of the elastic and piezoelectric tensors. For energy band calculations, the spin orbital coupling (SOC) is also taken into account due to containing early transition metal. Projector-augmented wave pseudopotentials are used with a cutoff energy of 500 eV for plane-wave expansions. A vacuum spacing of more than 20 \AA is adopted to prevent any interactions between the adjacent periodic images of the 2D monolayers. The total energy convergence criterion is set to 10^{-8} eV, and the atomic positions are optimized until all components of the forces on each atom are reduced to values less than $0.0001 \text{ eV} \cdot \text{\AA}^{-1}$. We calculate the coefficients of elastic stiffness tensor C_{ij} by using strain-stress relationship (SSR) and the piezoelectric stress coefficients e_{ij} by DFPT method²⁶. A Monkhorst-Pack mesh of $15 \times 15 \times 1$ in the first Brillouin zone is sampled for C_{ij} , and $9 \times 16 \times 1$ for e_{ij} . The 2D elastic coefficients C_{ij}^{2D} and piezoelectric stress coefficients e_{ij}^{2D} have been renormalized by the length of unit cell along z direction (Lz): $C_{ij}^{2D} = Lz C_{ij}^{3D}$ and $e_{ij}^{2D} = Lz e_{ij}^{3D}$. However, the d_{ij} is independent of Lz .

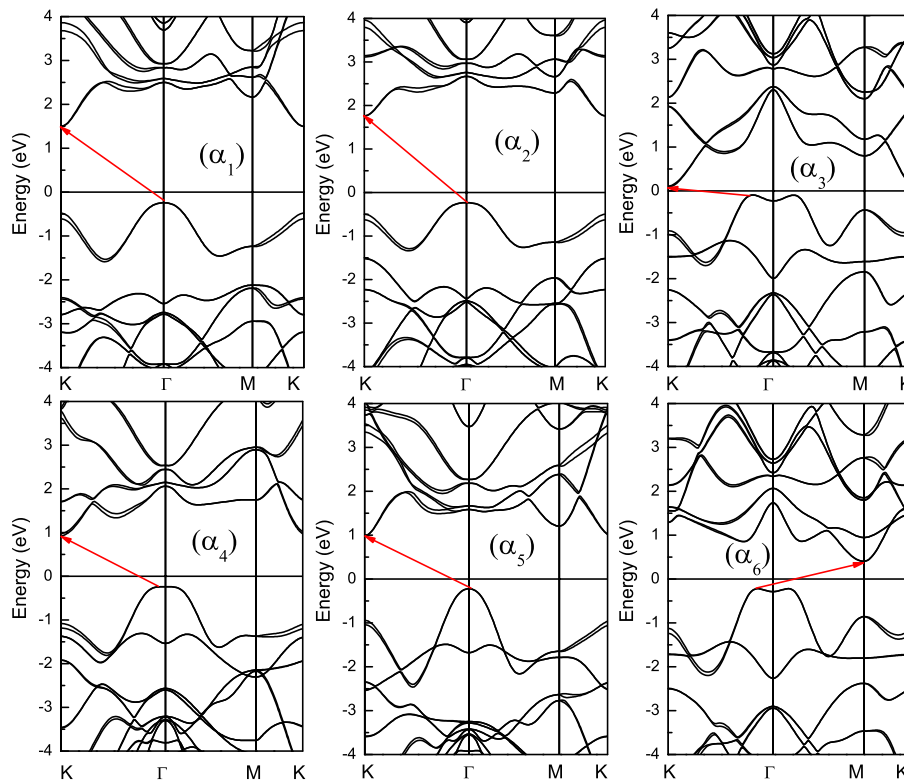


FIG. 2. (Color online) The energy band structures of α_i - ($i=1$ to 6) MoSi_2N_4 using GGA+SOC, and the VBM and CBM are connected by red arrow.

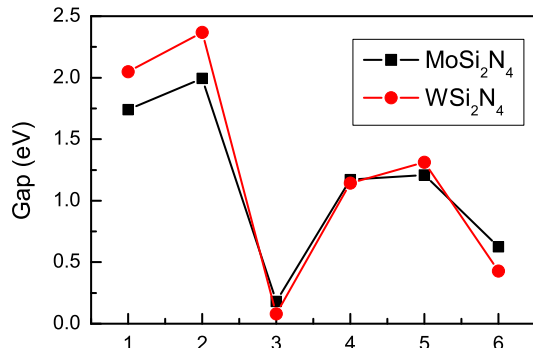


FIG. 3. (Color online) The energy band gaps of α_i - ($i=1$ to 6) MoSi_2N_4 and WSi_2N_4 using GGA+SOC.

TABLE II. The d_{11} of α_i - ($i=1$ to 6) MSi_2N_4 ($M=\text{Mo}$ and W) using GGA (pm/V).

Name	α_1	α_2	α_3	α_4	α_5	α_6
MoSi_2N_4	1.15	0.65	0.34	-1.98	3.53	1.32
WSi_2N_4	0.78	0.25	-0.07	-2.05	2.91	0.88

III. SYMMETRY ANALYSIS

The piezoelectric stress tensors e_{ijk} and strain tensor d_{ijk} is defined as:

$$e_{ijk} = \frac{\partial P_i}{\partial \varepsilon_{jk}} = e_{ijk}^{elc} + e_{ijk}^{ion} \quad (1)$$

and

$$d_{ijk} = \frac{\partial P_i}{\partial \sigma_{jk}} = d_{ijk}^{elc} + d_{ijk}^{ion} \quad (2)$$

where P_i , ε_{jk} and σ_{jk} are polarization vector, strain and stress, respectively. The e_{ijk}^{elc} (d_{ijk}^{elc}) is the clamped-ion piezoelectric tensors resulting from the pure electronic contribution. The relaxed-ion piezoelectric tensors e_{ijk} (d_{ijk}) is obtained from the sum of ionic and electronic contributions. The d_{ijk} can be connected with e_{ijk} by the elastic stiffness tensor C_{ijkl} . By employing the frequently used Voigt notation (11 \rightarrow 1, 22 \rightarrow 2, 33 \rightarrow 3, 23 \rightarrow 4, 31 \rightarrow 5 and 12 \rightarrow 6), the elastic tensor C_{ijkl} , piezoelectric tensors e_{ijk} and d_{ijk} become into C_{ij} (6×6 matrix), e_{ij} (3×6 matrix) and d_{ij} (3×6 matrix). The symmetry of crystal structure will further reduce the number of independent C_{ij} , e_{ij} and d_{ij} tensors.

By intercalating MoS_2 -type MZ_2 monolayer into InSe-type A_2Z_2 monolayer, six α_i and six β_i ($i=1$ to 6) MA_2Z_4 monolayers can be constructed²². The six α_i have the

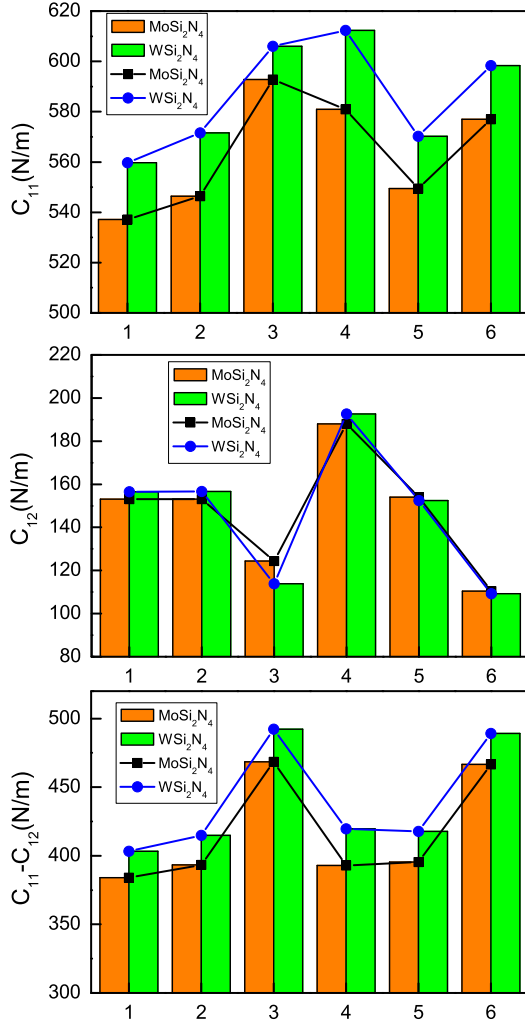


FIG. 4. (Color online) The elastic constants C_{ij} of α_i - ($i=1$ to 6) MoSi_2N_4 and WSi_2N_4 .

same $P\bar{6}m2$ space group due to inserting 2H- MoS_2 -type MZ_2 monolayer into α -InSe-type A_2Z_2 double layers, which break inversion symmetry. The six β_i are built by intercalating 1T- MoS_2 -type MZ_2 monolayer into β -InSe-type A_2Z_2 double layers with the same $P\bar{3}m1$ space group, which keep inversion symmetry. Therefore, α_i - ($i=1$ to 6) MA_2Z_4 monolayers are piezoelectric.

The six α_i geometric structures of the MA_2Z_4 monolayer are plotted in Figure 1. All considered six α_i crystal structures have the same $\bar{6}m2$ point group. Only the in-plane piezoelectric effect is allowed in monolayer α_i - ($i=1$ to 6) MA_2Z_4 , when a uniaxial in-plane strain is applied. For 2D semiconductors, in general, in-plane stresses and strains are only allowed, while the out-of-plane is strain/stress free⁷⁻⁹. And then the e_{ij} , d_{ij} and C_{ij} can be written as:

$$\begin{pmatrix} e_{11} & -e_{11} & 0 \\ 0 & 0 & -e_{11} \\ 0 & 0 & 0 \end{pmatrix} \quad (3)$$

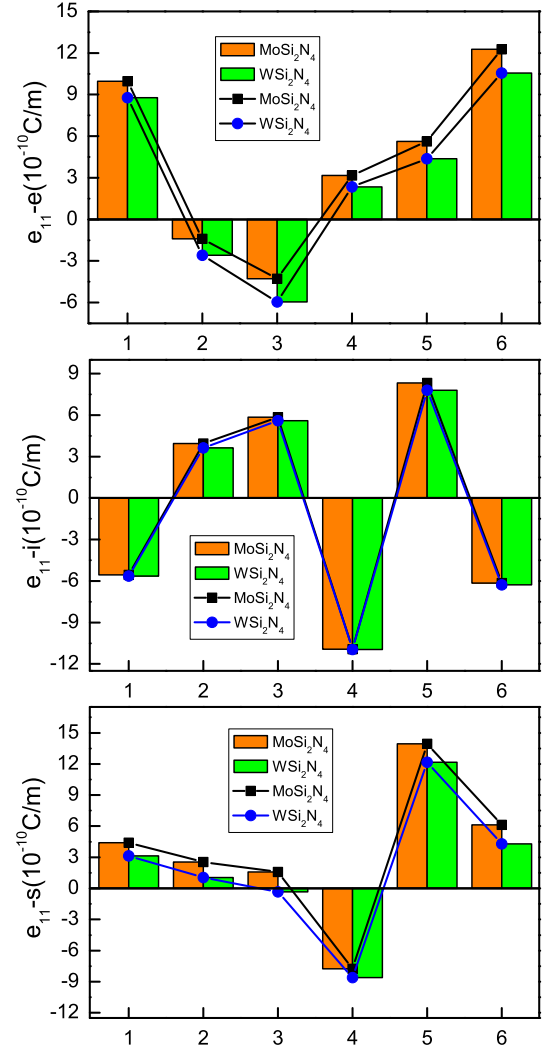


FIG. 5. (Color online) The piezoelectric stress coefficients e_{11} , the ionic contribution and electronic contribution to e_{11} of α_i - ($i=1$ to 6) MoSi_2N_4 and WSi_2N_4 .

$$\begin{pmatrix} d_{11} & -d_{11} & 0 \\ 0 & 0 & -2d_{11} \\ 0 & 0 & 0 \end{pmatrix} \quad (4)$$

$$\begin{pmatrix} C_{11} & C_{12} & 0 \\ C_{12} & C_{11} & 0 \\ 0 & 0 & \frac{C_{11}-C_{12}}{2} \end{pmatrix} \quad (5)$$

The forms of these piezoelectric and stiffness constants are the same as those for TMD monolayers^{7,9} due to the same point group. By $e_{ik}=d_{ij}C_{jk}$, the only in-plane d_{11} is found to be:

$$d_{11} = \frac{e_{11}}{C_{11} - C_{12}} \quad (6)$$

TABLE III. The optimized lattice constants of α_i - ($i=1$ to 2) MA_2Z_4 ($M=Cr, Mo$ and W ; $A=Si$ and Ge ; $Z=N$ and P) expect $CrGe_2N_4$ using GGA (\AA).

Name	CrSi ₂ N ₄	MoSi ₂ N ₄	WSi ₂ N ₄	MoGe ₂ N ₄	WGe ₂ N ₄	CrSi ₂ P ₄	MoSi ₂ P ₄	WSi ₂ P ₄	CrGe ₂ P ₄	MoGe ₂ P ₄	WGe ₂ P ₄
α_1	2.84	2.91	2.91	3.02	3.02	3.42	3.47	3.47	3.50	3.54	3.54
α_2	2.84	2.90	2.90	3.01	3.01	3.41	3.45	3.46	3.49	3.53	3.53

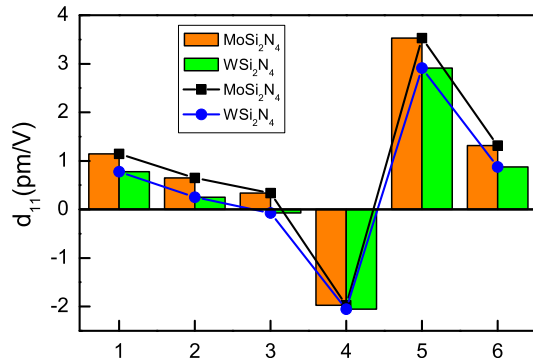


FIG. 6. (Color online) The piezoelectric strain coefficients d_{11} of α_i - ($i=1$ to 6) $MoSi_2N_4$ and WSi_2N_4 .

IV. MAIN CALCULATED RESULTS

Firstly, we discuss the structural relation among six α_i crystal structures of MA_2Z_4 . According to the relative positions of M and A atoms, the six α_i crystal structure can be divided into three categories: A (α_1, α_2), B (α_3, α_4) and C (α_5, α_6). The different categories can be connected by translation operation. The α_3 can be attained by translating A_2Z_2 double layers of α_2 along the green line of top view of α_2 in Figure 1 with the transfixion of MZ_2 monolayer. The α_6 can be attained from α_4 by similar translation operation. The different structures in the same category can be related by mirror or rotation operations. The α_2 can be built by mirroring A_2Z_2 double layers of α_1 with respect to the vertical surface defined by two green lines of top and side views of α_1 . The α_4 (α_6) can be constructed by rotating the A_2Z_2 double layers of α_3 (α_5) with $\pi/3$ along the vertical axis defined by linking two A atoms.

It has been proved that monolayer MA_2Z_4 ($M=Cr, Mo$ and W ; $A=Si$ and Ge ; $Z=N$ and P) expect $CrGe_2N_4$ with 34 VEC are non-magnetic with α_1 or α_2 crystal structure, and are both dynamically and thermodynamically²². A piezoelectric material should be a semiconductor for prohibiting current leakage. Only MSi_2N_4 ($M=Mo$ and W) monolayers are semiconductors for all six α_i crystal structures. So, we mainly study the structure effect on intrinsic piezoelectricity of MSi_2N_4 ($M=Mo$ and W). The structural parameters of α_i - ($i=1$ to 6) MSi_2N_4 ($M=Mo$ and W) are optimized, and the lattice constants are listed in Table I. It is found that the lattice constants between $MoSi_2N_4$ and WSi_2N_4 with the same phase are almost the same. The size of these lattice constants can also be

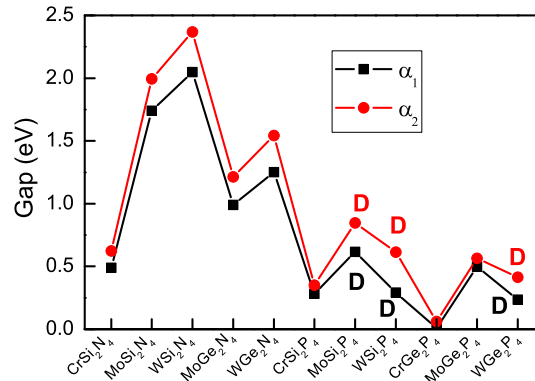


FIG. 7. (Color online) The energy band gaps of α_i - ($i=1$ to 2) MA_2Z_4 ($M=Cr, Mo$ and W ; $A=Si$ and Ge ; $Z=N$ and P) expect $CrGe_2N_4$ using GGA+SOC. The direct band gap is marked by "D", and the unmarked one is indirect band gap.

classified into A, B and C, which declare that the relative positions of M and A atoms determine lattice constants.

Next, we use optimized crystal structures to investigate their electronic structures. Although the SOC has little effects on the energy band gaps of MSi_2N_4 ($M=Mo$ and W) monolayers, the SOC can produce observed spin-orbit splitting in the valence bands at K point²³. Because the energy band outlines between $MoSi_2N_4$ and WSi_2N_4 are very similar, only the energy bands of α_i - ($i=1$ to 6) $MoSi_2N_4$ are shown in Figure 2 using GGA+SOC. It is clearly seen that they all are indirect gap semiconductors, and the gap range is 0.18 eV to 1.99 eV. The position of conduction band minimum (CBM) for all six α_i is at K point, except for α_6 at M point. The valence band maximum (VBM) of α_1, α_2 and α_5 is at Γ point, while the one of α_3, α_4 and α_6 is slightly off Γ point, and at one point along the Γ -K line. The energy band gaps of α_i - ($i=1$ to 6) $MoSi_2N_4$ and WSi_2N_4 using GGA+SOC are plotted Figure 3. It is clearly seen that the structural dependence of band gap of WSi_2N_4 is the same with one of $MoSi_2N_4$, and the gap ranges from 0.08 eV to 2.37 eV. Therefore, it is very effective to tune the electronic structures of MSi_2N_4 ($M=Mo$ and W) monolayers by translating or rotating Si_2N_2 bilayer.

To calculate the d_{11} , two independent elastic stiffness coefficients (C_{11} and C_{12}) of α_i - ($i=1$ to 6) $MoSi_2N_4$ and WSi_2N_4 are attained by SSR, which are plotted in Figure 4, together with C_{11} - C_{12} . For six structures, all calculated elastic coefficients of $MoSi_2N_4$ and WSi_2N_4 satisfy the Born stability criteria³², which means that they all

TABLE IV. The d_{11} of α_i - ($i=1$ to 2) MA_2Z_4 ($\text{M}=\text{Cr, Mo}$ and W ; $\text{A}=\text{Si}$ and Ge ; $\text{Z}=\text{N}$ and P) expect CrGe_2N_4 using GGA (pm/V).

Name	CrSi_2N_4	MoSi_2N_4	WSi_2N_4	MoGe_2N_4	WGe_2N_4	CrSi_2P_4	MoSi_2P_4	WSi_2P_4	CrGe_2P_4	MoGe_2P_4	WGe_2P_4
α_1	1.24	1.15	0.78	1.85	1.31	6.03	4.91	4.16	6.12	5.27	4.36
α_2	1.42	0.65	0.25	0.75	0.26	3.96	2.64	1.65	5.06	3.87	2.77

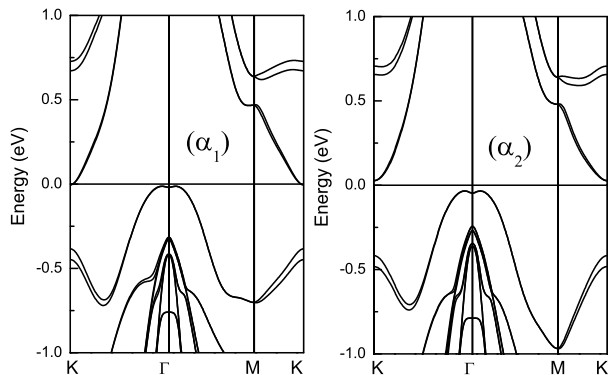


FIG. 8. The energy band structures of α_i - ($i=1$ to 2) CrGe_2P_4 using GGA+SOC.

are mechanically stable. Similar structural dependence of C_{11} , C_{12} and $C_{11}-C_{12}$ can be observed between MoSi_2N_4 and WSi_2N_4 . It is found that the C_{12} of two structures in the same category are very close, if the two structures are connected by mirror operation (α_1 and α_2). However, the C_{12} has obvious difference for two structures related by rotation operation (α_3 and α_4 or α_5 and α_6). The α_4 (α_5) has the larger C_{12} than α_3 (α_6). Between α_4 (α_3) and α_5 (α_6), the difference is only the position of Si atom. It is found that the $C_{11}-C_{12}$ of α_1 , α_2 , α_4 and α_5 are close, and α_3 and α_6 have the larger $C_{11}-C_{12}$, which is against the d_{11} according to Equation 6. These elastic stiffness coefficients are very larger than ones of TMD monolayers^{7,9}, which indicates that MoSi_2N_4 and WSi_2N_4 are not easy to be deformed.

Another key physical quantity e_{11} of α_i - ($i=1$ to 6) MoSi_2N_4 and WSi_2N_4 are calculated to attain d_{11} . Their piezoelectric coefficients e_{11} along with the ionic contribution and electronic contribution to e_{11} are shown Figure 5. It is clearly seen that the similar structural dependence between MoSi_2N_4 and WSi_2N_4 can be observed. It is found that the ionic contribution of two structures connected by mirror or rotation operations in the same category has opposite sign. In the different category, the ionic contribution of two structures connected by translation operation has the same sign. Calculated results show that the ionic contribution and electronic contribution have opposite sign for all α_i except α_5 . For A and B categories, the electronic contribution has similar structural dependence with ionic contribution. In the C category, the rotation operation gives rise to the identical signs for electronic contribution from α_6 to α_5 . In considered six structures, the e_{11} of α_5 has the largest value, which is

due to superposed ionic contribution and electronic contribution. The e_{11} with α_5 phase is 13.95×10^{-10} C/m for MoSi_2N_4 , and 12.17×10^{-10} C/m for WSi_2N_4 . These e_{11} are very larger than ones of 2D TMD, metal oxides, III-V semiconductor and Janus TMD materials^{2,7,9}. The e_{11} of experimentally synthesized α_1 - MoSi_2N_4 and WSi_2N_4 is 4.40×10^{-10} C/m and 3.14×10^{-10} C/m, which are comparable to that of most 2D materials, such as TMD and Janus TMD materials^{2,7,9}. Using the calculated $C_{11}-C_{12}$ and e_{11} , the d_{11} can be attained according to Equation 6, which are shown in Figure 6. From α_1 to α_6 , the d_{11} and e_{11} show very analogical structural dependence. For α_5 phase, the d_{11} has the largest value of 3.53 pm/V for MoSi_2N_4 , and 2.91 pm/V for WSi_2N_4 . For experimentally synthesized α_1 - MoSi_2N_4 and WSi_2N_4 , the d_{11} is 1.14 pm/V and 0.78 pm/V, which are smaller than that of 2D TMD^{7,9} due to very large $C_{11}-C_{12}$. The related d_{11} are listed in Table II.

For α_1 and α_2 phases, the monolayer MA_2Z_4 ($\text{M}=\text{Cr, Mo}$ and W ; $\text{A}=\text{Si}$ and Ge ; $\text{Z}=\text{N}$ and P) expect CrGe_2N_4 are all semiconductors using GGA+SOC. The energy band gaps of α_i - ($i=1$ to 2) MA_2Z_4 ($\text{M}=\text{Cr, Mo}$ and W ; $\text{A}=\text{Si}$ and Ge ; $\text{Z}=\text{N}$ and P) expect CrGe_2N_4 using GGA+SOC are plotted in Figure 7. It is found that the gap of CrGe_2P_4 is very small, and 0.008 eV for α_1 phase and 0.061 eV for α_2 phase. To unambiguously indicate them to be semiconductors, the energy band structures of α_i - ($i=1$ to 2) CrGe_2P_4 using GGA+SOC are shown in Figure 8. For the same material, the gap with α_2 phase is larger than one of α_1 phase. For MA_2N_4 , the gap increases with M from Cr to Mo to W, while the gap of MA_2P_4 firstly increases, and then decreases. Another reason is that their enthalpies of formation between α_1 and α_2 phases are very close²². So, we investigate the intrinsic piezoelectricity of the 11 kinds of materials with α_1 and α_2 phases. The optimize lattice constants are listed in Table III, and the lattice constants between α_1 and α_2 phases for the same material almost the same, which is because the α_1 and α_2 phases are in the same A class. With element changing from Cr to Mo to W, from Si to Ge, and from N to P, the lattice constants of both α_1 and α_2 phases increase, which is due to increasing atomic radius.

The elastic constants C_{ij} of α_i - ($i=1$ to 2) MA_2Z_4 ($\text{M}=\text{Cr, Mo}$ and W ; $\text{A}=\text{Si}$ and Ge ; $\text{Z}=\text{N}$ and P) expect CrGe_2N_4 are plotted in Figure 9. For all studied materials, the $C_{11}-C_{12}$ with α_2 phase are larger than ones of α_1 phase, which is due to larger C_{11} and smaller C_{12} . The C_{ij} of α_i - ($i=1$ to 2) MA_2Z_4 containing P atom are very smaller than ones including N atom, which is favor of d_{11} .

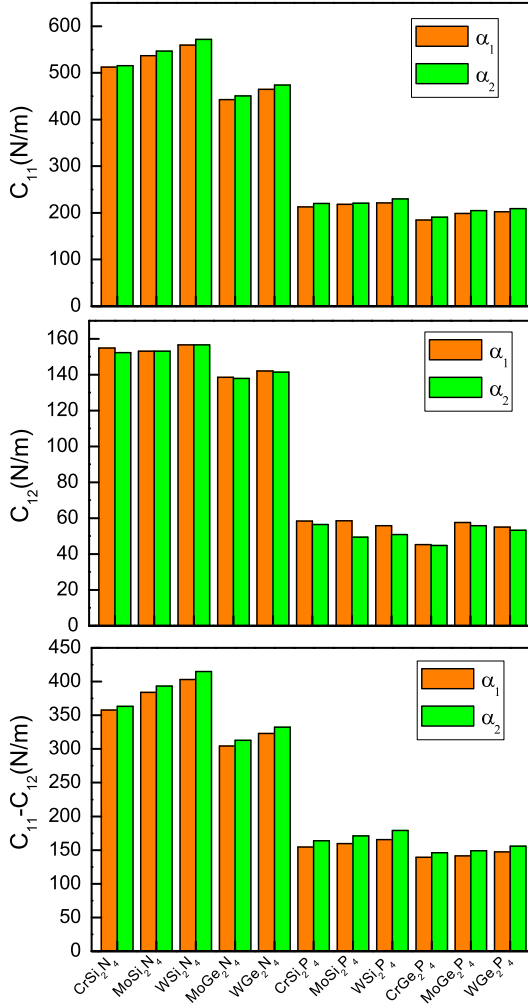


FIG. 9. (Color online) The elastic constants C_{ij} of α_i - ($i=1$ to 2) MA_2Z_4 ($M=\text{Cr}, \text{Mo}$ and W ; $A=\text{Si}$ and Ge ; $Z=\text{N}$ and P) expect CrGe_2N_4 .

The piezoelectric stress coefficients e_{11} of α_i - ($i=1$ to 2) MA_2Z_4 ($M=\text{Cr}, \text{Mo}$ and W ; $A=\text{Si}$ and Ge ; $Z=\text{N}$ and P) expect CrGe_2N_4 together with the ionic contribution and electronic contribution to e_{11} are shown in Figure 10. When M changes from Cr to Mo to W with the same A and Z atoms, the electronic contribution of MA_2Z_4 with α_1 phase decreases, while the one of α_2 phase changes toward more negative value. It is found that the electronic contribution (absolute value) of all MA_2Z_4 with α_2 phase is smaller than one of α_1 . The ionic contribution of all materials with α_2 phase is positive, which is the same with the electronic contribution of α_1 . With M from Cr to Mo to W , the ionic contribution of MA_2Z_4 of α_2 phase with the same A and Z atoms decreases, while the one of α_1 phase changes toward more negative value except for CrSi_2N_4 . It is clearly seen that the e_{11} of all materials are positive values. The e_{11} of MA_2Z_4 containing P atom with the same M and A atoms is larger than one including N atom for both α_1 and α_2 phases. For α_1 phase, the

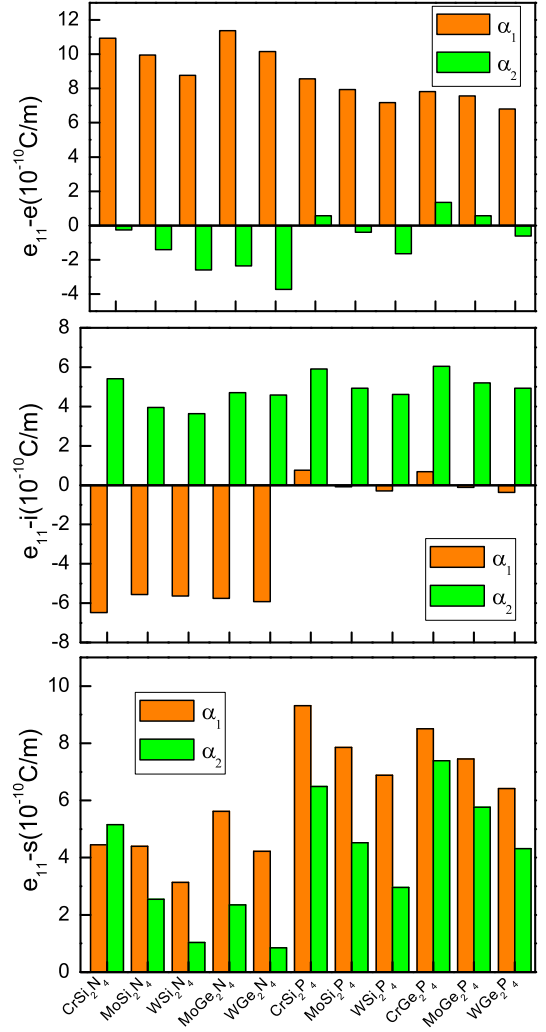


FIG. 10. (Color online) The piezoelectric stress coefficients e_{11} , the ionic contribution and electronic contribution to e_{11} of α_i - ($i=1$ to 2) MA_2Z_4 ($M=\text{Cr}, \text{Mo}$ and W ; $A=\text{Si}$ and Ge ; $Z=\text{N}$ and P) expect CrGe_2N_4 .

e_{11} ranges from 3.14×10^{-10} C/m to 9.31×10^{-10} C/m, and the whole range for α_2 phase is 0.85×10^{-10} C/m to 7.39×10^{-10} C/m.

Finally, the piezoelectric strain coefficients d_{11} of α_i - ($i=1$ to 2) MA_2Z_4 ($M=\text{Cr}, \text{Mo}$ and W ; $A=\text{Si}$ and Ge ; $Z=\text{N}$ and P) expect CrGe_2N_4 are plotted in Figure 11. The related d_{11} are also summarized in Table IV. For α_1 phase, the range of d_{11} is 0.78 pm/V to 6.12 pm/V, and the range changes from 0.25 pm/V to 5.06 pm/V for α_2 phase. The change trend of d_{11} as a function of material is very similar with one of e_{11} . It is clearly seen that monolayer MA_2Z_4 containing P atom have more excellent piezoelectric response due to high d_{11} . The most d_{11} of them are larger than $d_{33} = 3.1$ pm/V of familiar bulk piezoelectric wurtzite GaN^{33} . So, it is highly recommended to synthesize monolayer MA_2Z_4 containing P atom, such as α_1 - CrSi_2P_4 , α_1 - MoSi_2P_4 , α_1 - CrGe_2P_4 , α_1 - MoGe_2P_4 and α_2 - CrGe_2P_4 .

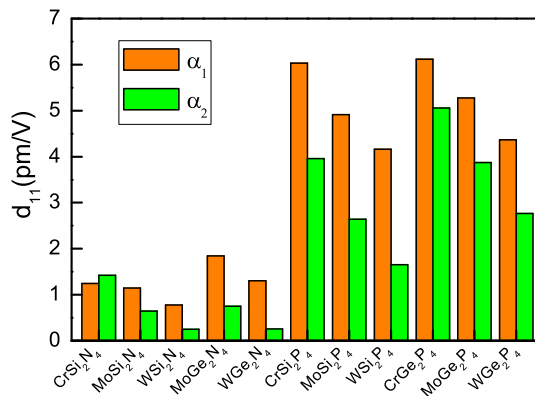


FIG. 11. (Color online) The piezoelectric strain coefficients d_{11} of α_i - ($i=1$ to 2) MA₂Z₄ (M=Cr, Mo and W; A=Si and Ge; Z=N and P) expect CrGe₂N₄.

V. CONCLUSION

We have demonstrated strong structure effect on intrinsic piezoelectricity in septuple-atomic-layer MSi₂N₄ (M=Mo and W) through first-principles simulations. The same structural dependence on d_{11} and e_{11} , together with the ionic and electronic contributions to e_{11} between MoSi₂N₄ and WSi₂N₄ monolayers is found, and the α_5 phase has large piezoelectric coefficients. The intrinsic piezoelectricity of monolayer MA₂Z₄ (M=Cr, Mo and W; A=Si and Ge; Z=N and P) with α_1 and α_2 phases expect CrGe₂N₄ are explored, and the monolayer MA₂P₄

have more stronger piezoelectric polarization than monolayer MA₂Z₄ including N atom. The largest d_{11} among MA₂N₄ materials only is 1.85 pm/V, and the largest d_{11} of MA₂P₄ is up to 6.12 pm/V. Among the studied 22 materials, the d_{11} of monolayer α_1 -CrSi₂P₄, α_1 -MoSi₂P₄, α_1 -CrGe₂P₄, α_1 -MoGe₂P₄ and α_2 -CrGe₂P₄ are greater than or close to 5 pm/V. These d_{11} of MA₂P₄ compare favorably with piezoelectric coefficients of familiar bulk piezoelectrics such as α -quartz ($d_{11} = 2.3$ pm/V), wurtzite GaN ($d_{33} = 3.1$ pm/V) and wurtzite AlN ($d_{33} = 5.1$ pm/V)^{33,34}. Our works provide valuable guidance for experimental synthesis efforts, and hope our study will stimulate more research interest into MA₂Z₄ family, especially for its applications in piezoelectric field.

VI. DATA AVAILABILITY

The data that support the findings of this study are available from the corresponding author upon reasonable request.

ACKNOWLEDGMENTS

This work is supported by the Natural Science Foundation of Shaanxi Provincial Department of Education (19JK0809). We are grateful to the Advanced Analysis and Computation Center of China University of Mining and Technology (CUMT) for the award of CPU hours and WIEN2k/VASP software to accomplish this work.

- ¹ W. Wu and Z. L. Wang, Nat. Rev. Mater. **1**, 16031 (2016).
- ² L. Dong, J. Lou and V. B. Shenoy, ACS Nano, **11**, 8242 (2017).
- ³ Y. Xu, Z. Q. Li, C. Y. He, J. Li, T. Ouyang, C. X. Zhang, C. Tang and J. X. Zhong Appl. Phys. Lett. textbf116, 023103 (2020).
- ⁴ S. D. Guo, X. S. Guo, Z. Y. Liu and Y. N. Quan, J. Appl. Phys. **127**, 064302 (2020).
- ⁵ Y. Xu, Z. Q. Li, C. Y. He et al., Appl. Phys. Lett. **116**, 023103 (2020).
- ⁶ J. Tan, Y. H. Wang, Z. T. Wang et al., Nano Energy **65**, 104058 (2019).
- ⁷ M. N. Blonsky, H. L. Zhuang, A. K. Singh and R. G. Hennig, ACS Nano, **9**, 9885 (2015).
- ⁸ R. X. Fei, We. B. Li, J. Li and L. Yang, Appl. Phys. Lett. **107**, 173104 (2015)
- ⁹ K. N. Duerloo, M. T. Ong and E. J. Reed, J. Phys. Chem. Lett. **3**, 2871 (2012).
- ¹⁰ Y. Chen, J. Y. Liu, J. B. Yu, Y. G. Guo and Q. Sun, Phys. Chem. Chem. Phys. **21**, 1207 (2019).
- ¹¹ Y. G. Guo, H. Q. Zhu and Q. Wang, ACS Appl. Mater. Interfaces **11**, 1033 (2019).
- ¹² W. B. Li and J. Li, Nano Res. **8**, 3796 (2015).
- ¹³ Y. Guo, S. Zhou, Y. Z. Bai and J. J. Zhao, Appl. Phys. Lett. **110**, 163102 (2017).
- ¹⁴ S. D. Guo and S. Q. Wang, J. Phys. Chem. Solids **140**, 109375 (2020).
- ¹⁵ N. Jena, Dimple, S. D. Behere and A. D. Sarkar, J. Phys. Chem. C **121**, 9181 (2017).
- ¹⁶ Dimple, N. Jena, A. Rawat, R. Ahammed, M. K. Mohanta and A. D. Sarkar, J. Mater. Chem. A **6**, 24885 (2018).
- ¹⁷ W. Wu, L. Wang, Y. Li, F. Zhang, L. Lin, S. Niu, D. Chenet, X. Zhang, Y. Hao, T. F. Heinz, J. Hone and Z. L. Wang, Nature **514**, 470 (2014).
- ¹⁸ H. Zhu, Y. Wang, J. Xiao, M. Liu, S. Xiong, Z. J. Wong, Z. Ye, Y. Ye, X. Yin and X. Zhang, Nat. Nanotechnol. **10**, 151 (2015).
- ¹⁹ A. Y. Lu, H. Zhu, J. Xiao, C. P. Chuu, Y. Han, M. H. Chiu, C. C. Cheng, C. W. Yang, K. H. Wei, Y. Yang, Y. Wang, D. Sokaras, D. Nordlund, P. Yang, D. A. Muller, M. Y. Chou, X. Zhang and L. J. Li, Nat. Nanotechnol. **12**, 744 (2017).
- ²⁰ M. Dai, Z. Wang, F. Wang, Y. Qiu, J. Zhang, C. Y. Xu, T. Zhai, W. Cao, Y. Fu, D. Jia, Y. Zhou, and P. A. Hu, Nano Lett. **19**, 5416 (2019).
- ²¹ Y. L. Hong, Z. B. Liu, L. Wang et al., Science **369**, 670 (2020).
- ²² L. Wang, Y. P. Shi, M. F. Liu et al., arXiv:2008.02981 (2020).

- ²³ S. D. Guo, Y. T. Zhu and W. Q. Mu, arXiv:2008.05751 (2020).
- ²⁴ S. Li, W. K. Wu, X. L. Feng et al., arXiv:2009.13253 (2020).
- ²⁵ A. Bafekry, M. Faraji, D. M. Hoat et al., arXiv:2009.04267 (2020).
- ²⁶ X. Wu, D. Vanderbilt and D. R. Hamann, Phys. Rev. B **72**, 035105 (2005).
- ²⁷ P. Hohenberg and W. Kohn, Phys. Rev. **136**, B864 (1964); W. Kohn and L. J. Sham, Phys. Rev. **140**, A1133 (1965).
- ²⁸ G. Kresse, J. Non-Cryst. Solids **193**, 222 (1995).
- ²⁹ G. Kresse and J. Furthmüller, Comput. Mater. Sci. **6**, **15** (1996).
- ³⁰ G. Kresse and D. Joubert, Phys. Rev. B **59**, 1758 (1999).
- ³¹ J. P. Perdew, K. Burke and M. Ernzerhof, Phys. Rev. Lett. **77**, 3865 (1996).
- ³² R. C. Andrew, R. E. Mapasha, A. M. Ukpong and N. Chetty, Phys. Rev. B **85**, 125428 (2012).
- ³³ C. M. Lueng, H. L. W. Chan, C. Surya and C. L. Choy, J. Appl. Phys. **88**, 5360 (2000).
- ³⁴ R. Bechmann, Phys. Rev. **110**, 1060 (1958).